

PAPER

PIC simulations of post-pulse field reversal and secondary ionization in nanosecond argon discharges

To cite this article: H Y Kim *et al* 2018 *Plasma Sources Sci. Technol.* **27** 055011

View the [article online](#) for updates and enhancements.

Related content

- [Kinetic simulation of direct-current driven microdischarges in argon at atmospheric pressure](#)
Ya Zhang, Wei Jiang and Annemie Bogaerts
- [Numerical analyses of hydrogen plasma generation by nanosecond pulsed high voltages at near-atmospheric pressure](#)
Chieh-Wen Lo and Satoshi Hamaguchi
- [Advanced PIC-MCC simulation for the investigation of step-ionization effect in intermediate-pressure capacitively coupled plasmas](#)
Jin Seok Kim, Min Young Hur, Chang Ho Kim *et al.*

PIC simulations of post-pulse field reversal and secondary ionization in nanosecond argon discharges

H Y Kim¹ , M Gołkowski¹, C Gołkowski², P Stoltz³, M B Cohen⁴ and M Walker⁵

¹ Department of Electrical Engineering, University of Colorado Denver, Denver, CO 80204, United States of America

² Super Pulse, Ithaca, NY 14850, United States of America

³ Tech-X Corporation, Boulder, CO 80303, United States of America

⁴ School of Electrical and Computer Engineering, Georgia Institute of Technology, Atlanta, GA 30313, United States of America

⁵ School of Aerospace Engineering, Georgia Institute of Technology, Atlanta, GA 30332, United States of America

E-mail: hoyoung.kim@ucdenver.edu

Received 5 February 2018, revised 17 April 2018

Accepted for publication 27 April 2018

Published 17 May 2018



CrossMark

Abstract

Post-pulse electric field reversal and secondary ionization are investigated with a full kinetic treatment in argon discharges between planar electrodes on nanosecond time scales. The secondary ionization, which occurs at the falling edge of the voltage pulse, is induced by charge separation in the bulk plasma region. This process is driven by a reverse in the electric field from the cathode sheath to the formerly driven anode. Under the influence of the reverse electric field, electrons in the bulk plasma and sheath regions are accelerated toward the cathode. The electron movement manifests itself as a strong electron current generating high electron energies with significant electron dissipated power. Accelerated electrons collide with Ar molecules and an increased ionization rate is achieved even though the driving voltage is no longer applied. With this secondary ionization, in a single pulse (SP), the maximum electron density achieved is 1.5 times higher and takes a shorter time to reach using 1 kV 2 ns pulse as compared to a 1 kV direct current voltage at 1 Torr. A bipolar dual pulse excitation can increase maximum density another 50%–70% above a SP excitation and in half the time of RF sinusoidal excitation of the same period. The first field reversal is most prominent but subsequent field reversals also occur and correspond to electron temperature increases. Targeted pulse designs can be used to condition plasma density as required for fast discharge applications.

Keywords: nanosecond pulse argon discharge, plasma characteristics, post-pulse secondary ionization, particle-in-cell simulation

1. Introduction

Nonthermal capacitively coupled plasmas have a wide range of applications in the areas of semiconductor fabrication, plasma lighting and display, biomedicine, and combustion processes [1–21]. A special class of applications, which includes plasma switches and displays, requires very fast plasma ionization times on the order of microseconds or even

nanoseconds [22–24]. In aerospace applications, nanosecond pulse discharges have been employed as flow control actuators, a source of ionization for non-equilibrium magneto hydrodynamic devices, and a means for enhancing ignition and combustion [25]. The motivation for the work herein is a novel dynamic plasma antenna, in which the conducting properties of a plasma column are changed on the order of the propagation time of a radiating surface wave. This type of

plasma antenna is very different from the more commonly described steady state plasma antenna [9, 26, 27], in which a sustained plasma column mimics a metallic conductor during radiation. The dynamic plasma antenna is divided into a series of segments, which can provide a conducting current path with the onset of a rapid pulsed plasma discharge and conversely can block a current path when the plasma is absent [28]. For this concept, it is critical that the plasma electron density is changed as fast as possible.

In all applications where precise discharge timing and evolution is required, the transient response of the plasma to an applied potential is of critical importance and stored energy in the plasma configuration can become an important parameter. Hill pioneered experiments using high voltage pulses in combination with a direct current (DC) sustainer [29]. More recently, Macharet *et al* [30] have explored optimization of the energy cost of sustaining plasmas and spatial dynamics of electric potential on nanosecond time scales. An important feature of transient plasma response to rapid potential change is an electric field reversal or ‘two-cathode’ effect in which stored energy in the bulk plasma region can lead to secondary ionization with termination of applied field. This effect was first reported by Raizer and Shneider [31] and was further investigated by Macharet *et al* [32].

We report a detailed numerical investigation of rapid electron density increase under pulsed voltage between two planar electrodes. The post-pulse field reversal process and resulting secondary ionization are explored in a full kinetic particle-in-cell (PIC) treatment that allows for accurate modeling of the low pressure regime (below 10 Torr for a gap of 1 cm) that can be a challenge for hydrodynamic approximations [30]. It is found that pulse duration and shape are important parameter for rapid ionization since they can allow stored energy accumulated in the initial discharge to be subsequently exploited.

2. Methods

Two parallel-plate electrodes separated by a 1 cm gap filled with argon (Ar) gas at a pressure of 1 Torr are modeled. Due to the low pressures and short time scales of interest (<20 ns), fluid models based on assumptions of Maxwellian velocity distributions can be inaccurate and kinetic models are most appropriate [4, 6]. We employ a one-dimensional (1d3v) PIC simulation (XPDP1 [4, 6–8]) with a Monte Carlo collision (MCC) method, which is self-consistent and fully kinetic. The secondary electron coefficient for Ar ions are set to 0.1 [1, 3], whereas electrons are assumed to be perfectly absorbed at electrodes [4, 6–8, 13]. In steady state Ar plasma at 1 Torr, Ar metastable states need to be tracked because of their role in electron heating and ionization [33]. However, here we only track Ar ions and electrons for the transient response since on nanosecond time scales the densities of Ar metastable states are very low compared with neutral Ar molecules. Electron energy is tracked by taking into account elastic, cumulative excitation and ionization cross sections. Electrons, charged

and neutral particles are initially uniformly distributed in the simulation domain and in velocity space. The positions, velocities, and energies of these particles are estimated by weighting values known at the grid points and these are updated by solving MCC and the Newton–Lorentz equation. The MCC uses a null collision method with energy dependent cross sections [34, 35]. Electrons can undergo elastic ($e + \text{Ar} \rightarrow e + \text{Ar}$), excitation ($e + \text{Ar} \rightarrow e + \text{Ar}^*$), and ionization ($e + \text{Ar} \rightarrow 2e + \text{Ar}^+$) collisions where Ar^* is a specie encompassing all excited states. Ions can undergo charge exchange ($\text{Ar}^+ + \text{Ar} \rightarrow \text{Ar} + \text{Ar}^+$) and scattering ($\text{Ar}^+ + \text{Ar} \rightarrow \text{Ar}^+ + \text{Ar}$) collisions [34]. Threshold energies for excitation and ionization are 11.55 and 15.76 eV, respectively. In the Newton–Lorentz equation, the electric field and potential are calculated with the charged densities by Poisson’s equation, obtained by combining Gauss’s law, with scalar potential [35]. The secondary electron coefficient for Ar ions are set to 0.1, whereas electrons are assumed to be perfectly absorbed at electrodes. In the simulations described below, the time step is always smaller than the shortest falling time of applied voltage (2×10^{-11} s) and inverse of collision frequency (1×10^{-10} s), and plasma frequency (5.8×10^{-10} s). The cell size is also smaller than maximum Debye length (5.254×10^{-6} m). The particle Courant–Friedrichs–Lewy condition $\nu\Delta t/\Delta x < 1$, where ν is the particle velocity, is satisfied for all particles [36].

The original motivation behind our simulation was to achieve the fastest possible increase in electron density to create a plasma conducting channel. This effort led to identification of the field reversal effect described in earlier works [31, 32, 37] as important in discharge rate optimization. Specifically, we have found that terminating the applied voltage and driving the electrodes with a finite duration voltage pulse achieves a higher density in shorter time scales than the DC voltage even if the magnitude of voltage in both cases is the same. We investigate this secondary ionization for pulses of 500 V with 3 ns duration and 1 kV and 2 kV with 2 ns duration. The shape of pulses in time is that of trapezoid consisting of rising, sustain, and falling time. Unless otherwise specified, the rising and falling times are each 1% of the total pulse duration.

3. Results

Figure 1(a) shows the transient response of electron density and average electron temperature for a 1 kV 2 ns pulse and 1 kV DC. In both cases, electron density sharply increases via collisional ionization up to 2 ns. After 2 ns, the electron density for the DC case saturates due to plasma shielding of the applied potential. Namely, a plasma bulk region occupies the majority of the inter-electrode spacing and the potential difference in this bulk region is almost zero as shown in figure 2(a). As the plasma shielding reduces the applied electric field, electrons experience primarily elastic collisions and electron density is saturated. This process can also be observed in the electron temperature, which is initially set to 0.001 eV for the seed population of 10^{15} m^{-3} . Until 0.8 ns,

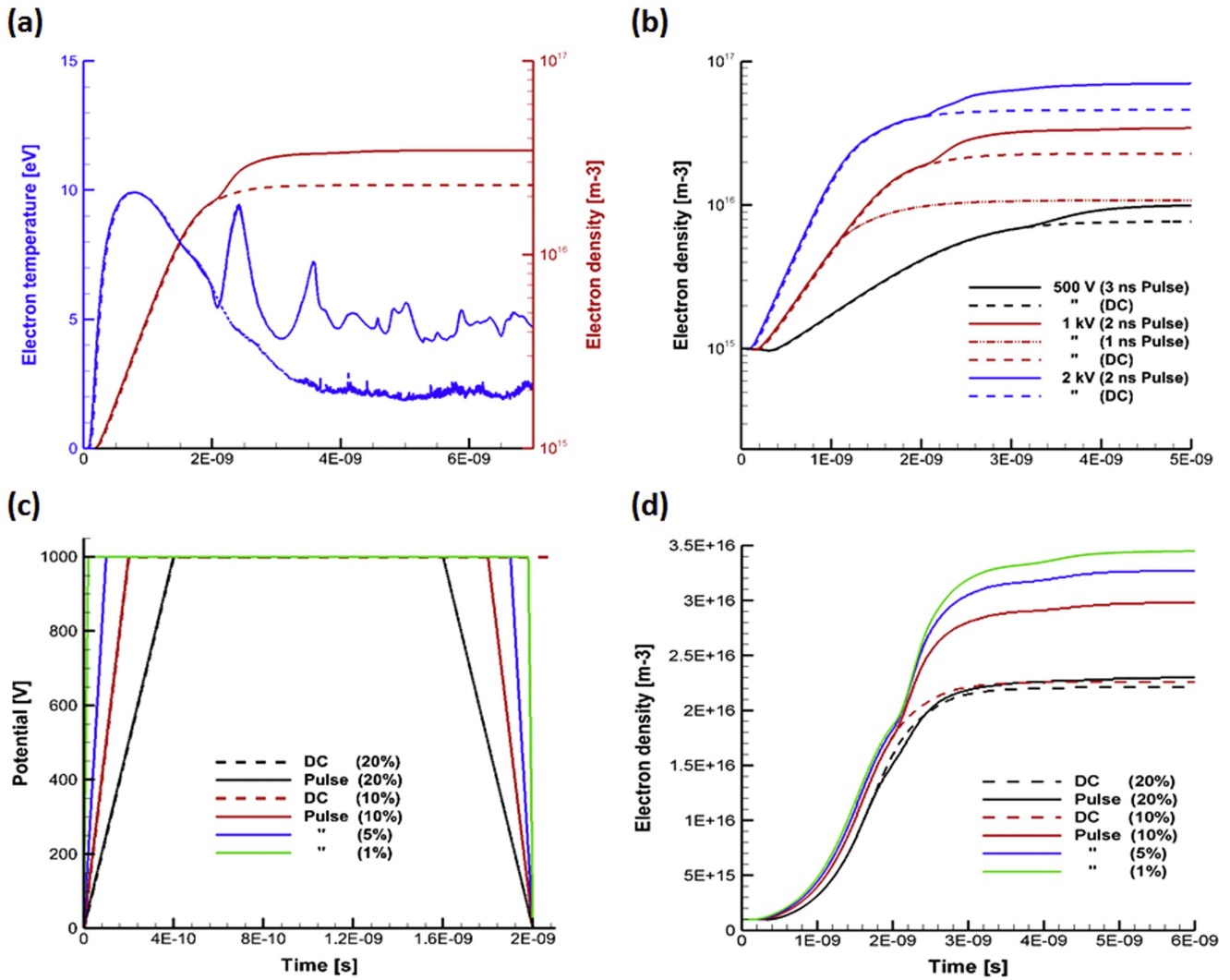


Figure 1. Transient response of averaged electron density and electron temperature in Ar plasma with different voltages and rise/fall times for DC and pulse cases. (a) Electron density and temperature for DC (dashed line) and pulsed cases (solid line). (b) Electron density with 500 V, 1 kV, and 2 kV DC and 3, 2, 1 ns pulse duration cases. Pulsed and DC waveforms in (a) and (b) have a 1% rise/fall time. (c) Definition of variable pulse rise/fall time for 2 ns pulse and (d) electron density results for/rise times of 1%, 5%, 10% and 20% for 2 ns pulsed and DC cases.

electron temperature increases reaching a maximum of 10 eV. Subsequently, electron temperature decreases because of inelastic collisions as the electron density continues to increase. The parameters for the case of the pulsed voltage depart from the DC case at 2 ns, the time of the pulse termination. At this time, the electron density shows an additional rise even though no external voltage is being applied and no extra energy is being supplied to the system. The average electron temperature exhibits two fluctuations, which are evidence of electron acceleration as the source of the additional ionization. Of practical importance is that with this secondary ionization process, the peak electron density achieved is higher than in the DC case. In other words, it takes a shorter time to reach a target electron density using a short pulse as compared to a DC voltage of the same magnitude.

Figure 1(b) shows electron density for values of applied voltage of 500 V, 1 kV, and 2 kV for DC and pulsed cases.

For the pulsed cases pulse durations of 1, 2, and 3 ns are modeled. For each of the different driven voltages, the electron density time-series have unexpected secondary increments except for the 1 ns pulse. The minimum duration of the pulse is a critical parameter. The secondary ionization increase only occurs if the pulse terminates after the bulk plasma region has formed, which is manifested by the saturation of electron density for the DC case. In the case of 1 kV 1 ns pulse, there is no secondary density increase and the final electron density is lower than that in 1 kV DC case. The secondary ionization can be triggered only after the plasma has accumulated capacitive energy in the bulk region. The amount of secondary ionization is also affected by the pulse rise and fall times. Figure 1(c) shows pulses with rise and fall times of 1%, 5%, 10% and 20% of the pulse duration. Figure 1(d) shows electron density for the pulsed case is 1.04 times higher than that for DC case when the rise/fall times are 20% of the pulse width. However, for a faster 10% rise/fall

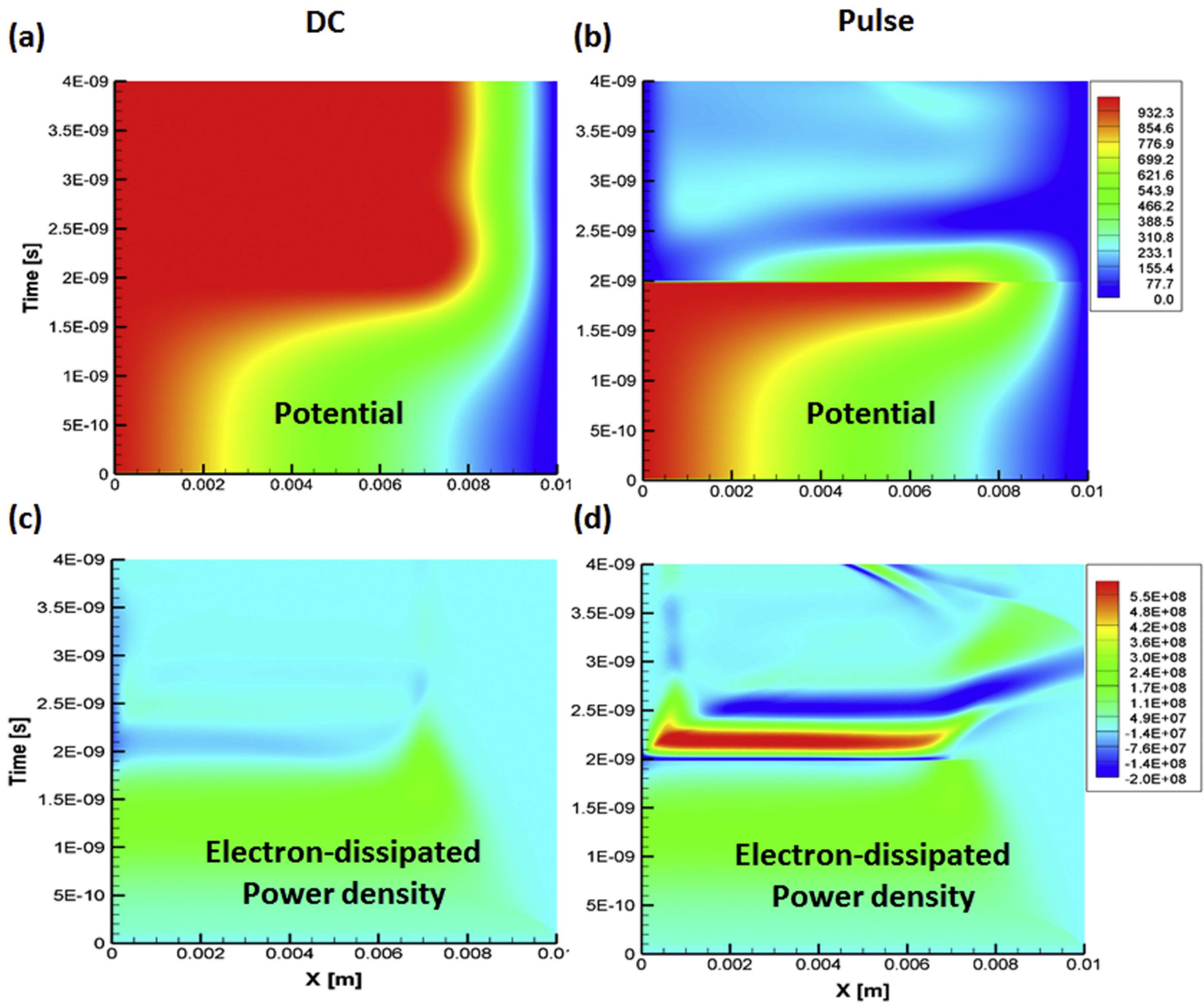


Figure 2. Time evolution of the potential and electron dissipated power density in Ar plasma with 1 kV DC and 1 kV 2 ns pulse cases. Potential for (a) DC and (b) pulse cases. Electron dissipated power density for (c) DC and (d) pulse cases.

time pulse, electron density is 1.3 times higher than that for DC case and 1.6 times higher than DC for a 1% rise/fall time. Sharper pulse terminations yield a greater amount of secondary ionization and higher plasma density.

To elucidate the electron and potential dynamics, figure 2 presents time and space plots of potential and resolved electron dissipated power density for a DC voltage in panels (a), (c) and pulsed voltage in panels (b), (d). Figures 2(a), (b) show the transient potential of DC and pulse cases. Before 2 ns, the potential spatial distribution of the two cases are identical as expected. For 1 Torr Ar driven with 1 kV across a 1 cm gap, the minimum time to create a bulk region is 2 ns as can be observed by the high potential from the anode filling 80% of the inter-electrode spacing except for a ~ 2 mm cathode sheath region on the right side of the plots. The electric field under these conditions is only significant near the cathode. At 2 ns, the driven voltage for the pulsed case is turned off. From 2 to 2.5 ns, in figure 2(b), there is a potential difference between the anode electrode and bulk region since

the anode has returned to zero potential. This potential leads to a reverse in the direction of the electric field, causing electrons in the bulk plasma and anode sheath regions to move toward the cathode. This electron movement manifests itself as an electron current with significant electron dissipated power ($J_e \cdot E$) as shown in figure 2(d) where J_e and E represent the electron current and electric field, respectively. In comparison with the DC case shown in figure 2(c), it is clear that the pulsed case exhibits higher dissipated power in the bulk region following pulse termination. This heating of electrons in the bulk region leads to the first post-pulse electron temperature increase that was seen in figure 1(a) at 2.5 ns. Electrons move from anode to cathode. From 2.5 to 3 ns, there is another reversal in electric as Ar ions outnumber electrons near the anode, but the opposite is true near the cathode. Under the influence of the electric field in this second reversal, electrons in the bulk and cathode sheath move toward the anode, leading to a high rate of inelastic collisions and loss of electron energy as seen in figure 2(d). This is the

reason for the second electron temperature decrease in figure 1(a) at 3 ns. After 3 ns, the electric field is in the direction from the anode to cathode sheath because of high electron density in the anode sheath. Electrons move toward the cathode. In the cathode sheath, electrons are heated, and it leads to a second electron temperature increase from 3 to 3.5 ns in figure 1(a). From 3.5 to 4 ns, electrons move back to the anode because of high Ar ions in anode sheath. This is manifested as a third electron temperature decrease seen in figure 1(a).

Since the post-pulse increase in electron density occurs without any energy contribution from the power supply, we can write an energy balance equation for the conditions after the pulse termination where the depletion of field energy stored in the plasma, $E_f(t)$, drives the remaining processes, which include changes in electron kinetic energy, $E_e(t)$, ionization, $E_i(t)$, excitation, $E_{ex}(t)$ and increase in kinetic energy of heavy species (ions and neutrals), $E_h(t)$:

$$-E_f(t) \approx E_e(t) + E_i(t) + E_{ex}(t) + E_h(t). \quad (1)$$

The equality in equation (1) is approximate since energy lost to the electrodes is not considered here making the expression accurate only for the bulk region. The terms in equation (1) can be evaluated from the numerical model as:

$$E_f = \text{area} * \sum_{i=0}^{n_c} \frac{\epsilon_0 (E_p^i)^2}{2} dx \quad (2)$$

$$E_e = \text{area} * q \sum_{i=0}^{n_c} \frac{3n_e^i T_e^i}{2} dx \quad (3)$$

$$E_i = k_{\text{ionz}} * q \sum_{t=0}^{t'} v_{\text{ionz}}^t dt \quad (4)$$

$$E_{ex} = k_{\text{ex}} * q \sum_{t=0}^{t'} v_{\text{ex}}^t dt, \quad (5)$$

where n_c , ϵ_0 , q , v are, respectively, number of cells, the permittivity of free space, elementary electric charge, and collision frequency. The parameters k_{ionz} and k_{ex} are threshold energy of ionization (15.76 eV) and excitation (11.5 eV). Electron energy is calculated by averaging velocities of all particles ($0.5m_e \langle v_e \rangle^2 = 1.5k_B T_e$) [13] and E_p in equation (2) is the electric field from plasma charge separation. Figure 3(a) shows the transient response of $E_f(t)$ for DC and pulsed cases. The field energy here is a stored energy in the bulk plasma and this can be seen to decrease abruptly at the pulse termination. Figure 3(b) shows the dynamics of all terms in equation (1) for the 1 kV 2 ns pulse from the time of pulse termination to 0.8 ns later. The sum of terms on the right hand side is shown to be equivalent to the negative of the field energy. The primary sink of field energy decrease is seen to be electron energy followed by ionization and excitation. $E_h(t)$ was found to be negligible due to the larger ion mass and is not plotted. As a further test of the validity of equation (1), the model was run with artificial decreases to the excitation scattering cross section which should lead to a decrease in $E_{ex}(t)$ and a corresponding increase in the remaining terms on the right hand side. Figure 3(c) shows that when the excitation cross section is decreased by a factor of

10 and 100, the electron kinetic energy $E_e(t)$, is seen to increase relative to the negative of field energy since energy transfer to excitation of the neutral atoms decreases. Figure 3(d) shows ratios of $\frac{E_e}{E_f}$ for different applied voltages and different excitation cross section values. In addition to the already mentioned increase of the ratio with decreasing cross section, $\frac{E_e}{E_f}$ also increases with applied voltage. The increase of $\frac{E_e}{E_f}$ with voltage is due to the energy dependence of the cross section, which peaks for electron temperature of 20–30 eV and then sharply decreases for higher energies. As the voltage increases from 500 V, the bulk electron energy is too high for excitation to play a significant role.

The key dynamic after the applied voltage pulse terminates is the oscillation of the electric field. The associated bulk electron motions are illustrated in figure 4, which shows electron density maps in time and space for different electron energy ranges. The left panels of figures 4(a), (c), (e), (g) show the time and space electron density for DC while the right panels (b), (d), (f), (h) for the pulsed (2 ns) case. Panels (a), (b) show total electron density, panels (c), (d) show the electron density for low-energies $T_e < 4$ eV, panels (e), (f) mid-energy $4 \text{ eV} < T_e < 10$ eV, and panels (g), (h) high-energy $T_e > 10$ eV. Before 2 ns, the profile of electron density is the same in DC and pulsed cases. In both cases, the cathode sheath is larger than the anode sheath as is typical for DC plasma discharges [1]. After 2 ns for the pulsed case, we see the electrons of all energies move from anode to cathode (to the right) and the creation of an anode sheath as shown in figure 4(b). The DC case in figure 4(a), also shows an increase in the anode sheath at 2 ns related to electron density saturation and plasma shielding of applied potential, but the anode sheath length in the pulsed case is longer. Figure 4(b) shows that the space profile of electron density also exhibits two fluctuations like was observed for electron temperature in figure 1 after 2 ns. In the low-energy range in figures 4(c), (d), the DC case has more electrons than the pulsed case for 2–2.5 ns since in the pulsed case the electrons are accelerated to higher energies. This corresponds to the average electron temperature increase seen in figure 1(a). After 3 ns, figure 4(c) shows that low-energy electrons of the DC case are gathering mainly in the bulk region on the cathode side. The bulk region has a 100 fold higher inelastic collision rate as compared to cathode sheath and consequently electrons lose energy with average temperature dropping. On the other hand, the majority of low-energy electrons in the pulsed case are closer to the anode as can be seen in figure 4(d). These low-energy electrons drive a subsequent reverse in electric field after 3 ns, which drives electron motion toward the cathode. Figures 4(d), (f), (h) show this electron movement takes place for all energy ranges. From 2.5 to 3 ns, there is a drop in low- and mid-energy electron numbers in figures 4(d), (f) but an increase of high-energy electron numbers in figure 4(h) when comparing the DC to pulsed case as a result of acceleration.

Since the secondary ionization is driven by a field reversal from the plasma itself, it is possible to amplify this effect by reversing the polarity of the applied voltage at the appropriate time, using what we call here a dual pulse (DP)

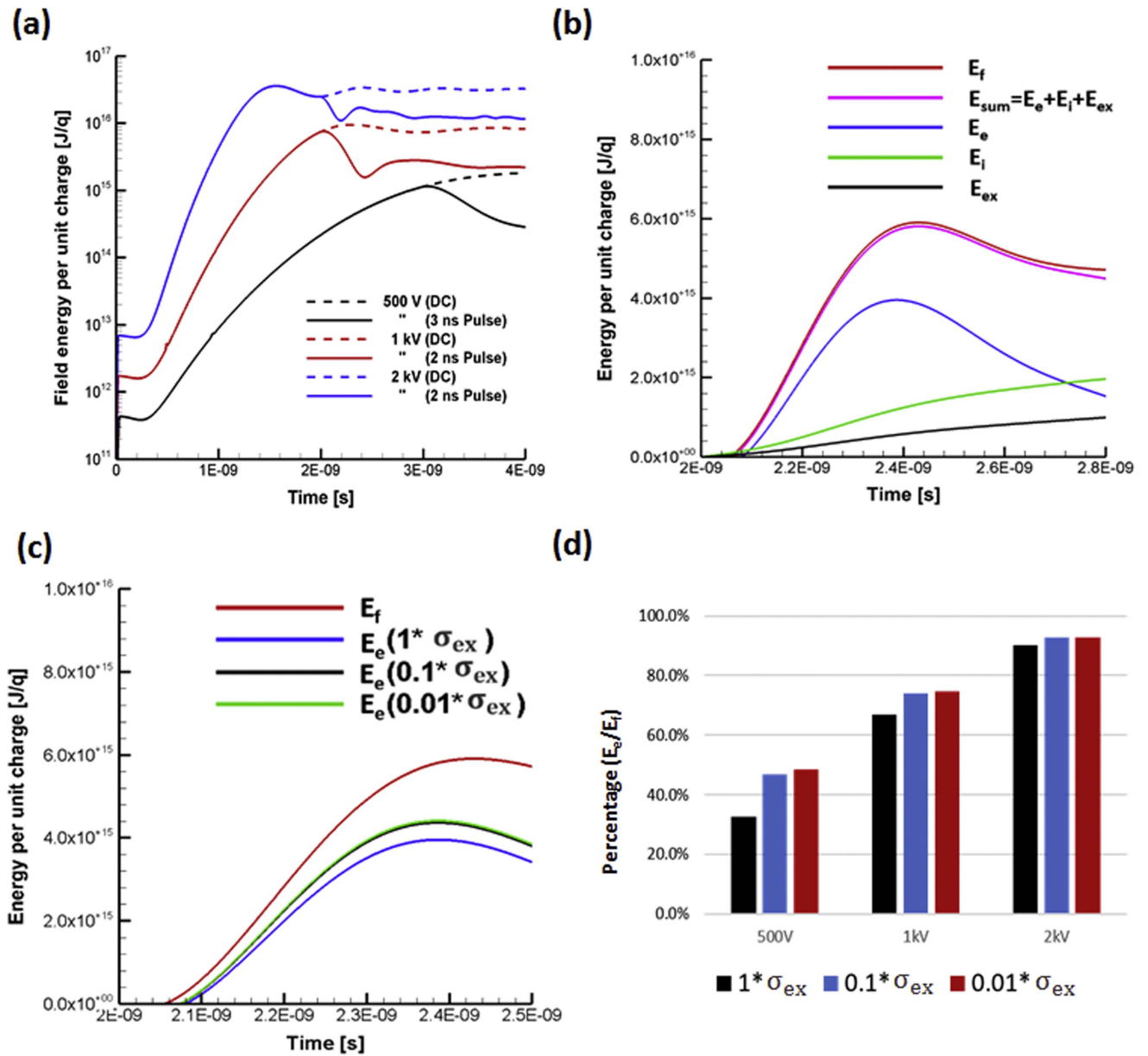


Figure 3. The transient response of field energy per unit charge, electron energy, energy loss by ionization and excitation with different voltages in DC and pulse cases. (a) Field energy per unit charge with 500 V, 1 kV and 2 kV of DC and pulse case. (b) energies per unit charge at 1 kV 2 ns pulse for decrease field energy, sum of energies with electron energy, energy loss by ionization and excitation. (c) energies per unit charge with different cross section of excitation. (d) Ratio of electron energy per decrease in field energy for different excitation cross sections.

excitation. Figure 5(a) shows the transient response of electron density and electron temperature for a 0.5 cm gap for a 1 kV, 1.5 ns single pulse (SP), DP and 1 kV DC voltage, the temporal shapes of which are shown in figure 5(c). In the cases of SP and DP, electron densities and temperatures increase after pulse termination. In the DP case, electron temperature increases until 33 eV and then decreases. Maximum electron density achieved is 3 times higher than that in the DC case. Figure 5(b) shows DC, SP, DP cases for 0.5, 1, and 2 cm gaps. Electron densities are higher with a smaller gap distance. Electron density in 0.5 cm is 2.18 times higher than that in a 2 cm gap. The amount of electron density difference between DC and SP is higher with a smaller gap. The

maximum electron density for SP 0.5 cm gap is 1.84 times higher than that in DC. The maximum electron density for DP 0.5 cm gap is 3.13 times higher than that in DC. The time for initial density to saturate and the bulk region to form decreases with smaller gap size and the associated higher applied electric field. This time to initial saturation is the time needed to ‘charge’ the field energy in the bulk region. We have also investigated a sinusoidal (RF) excitation corresponding to the DP waveform parameters of 1 kV amplitude at 0.33 GHz as shown in figure 5(c). Figure 5(d) shows DC, SP, and DP with 0.5, 1.5, 2 ns pulses and RF cases all for 0.5 cm gap. The density for the 0.5 ns SP is lower than that in the DC case, meaning that there was insufficient time for the plasma

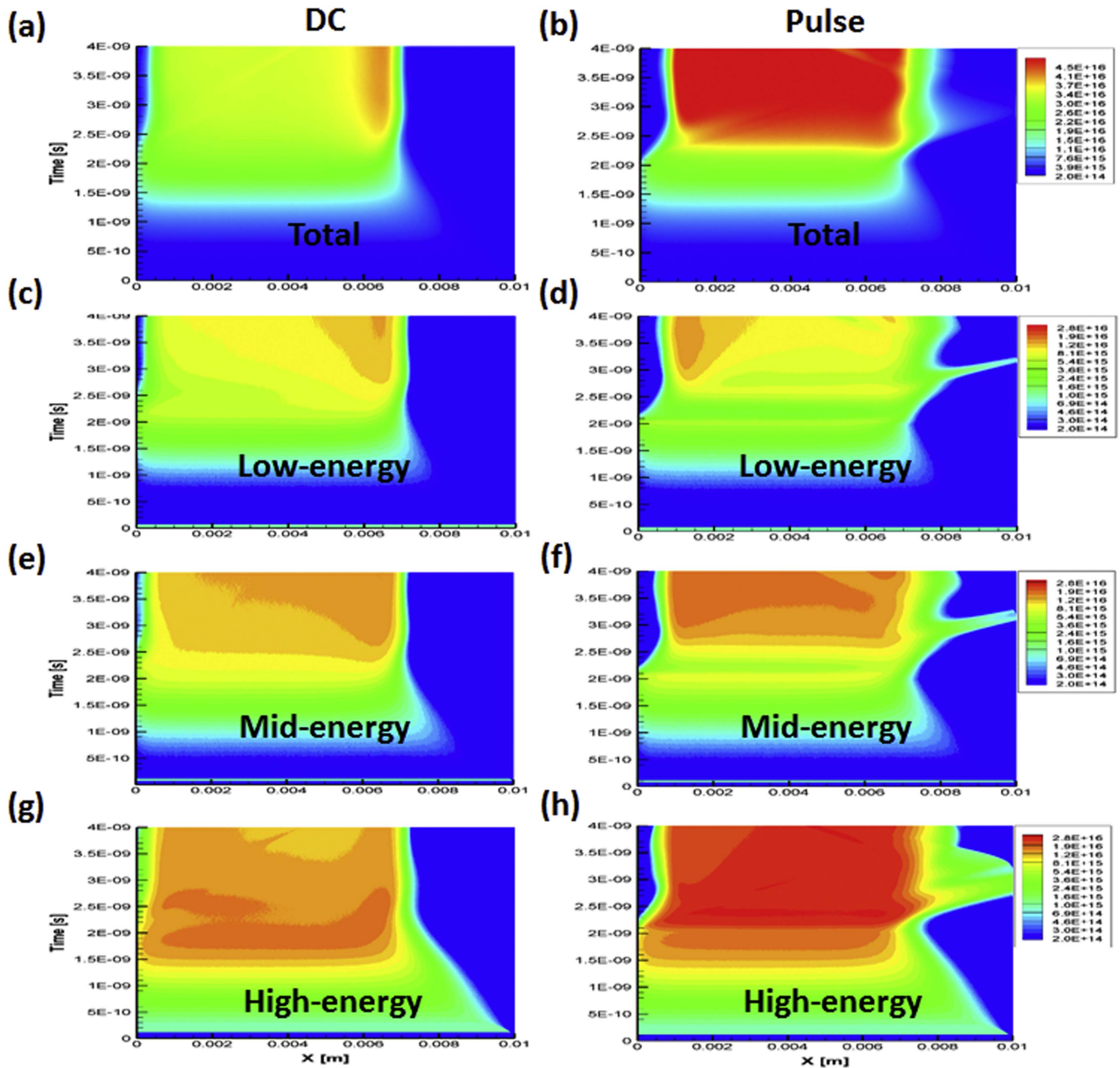


Figure 4. Time evolution of the electron density in Ar plasma with 1 kV DC and 1 kV 2 ns pulse cases. (a), (b) Total electron density. (c), (d) Electron density with low-energy $e < 4$ eV in log scale. (e), (f) Electron density with mid-energy $4 < e < 10$ eV in log scale. (g), (h) Electron density with high-energy $e > 10$ eV.

to be charged with field energy in the bulk region. Densities in 1.5 and 2 ns eventually reach the same maximum values. In other words, stored field energy reaches a maximum after 1.5 ns. Electron density in the RF case is seen to reach a maximum level similar to the DP case. However, the maximum electron density in RF occurs at 4 ns but in DP is 2 ns, so discharge time can be reduced by 50% with steep pulses.

4. Summary and discussion

Secondary ionization is induced by voltage pulse termination driven by the stored energy in the bulk plasma region. In the

SP scenario, after pulse termination, electron motion and energy undergo oscillations. Under the influence of the initially reversed electric field, electrons in the bulk plasma and anode sheath regions move toward the cathode. This electron movement manifests itself as a strong electron current, generating high electron energies with significant electron dissipated power. There are high-energy electrons at both electrodes and the center. High-energy electrons collide with Ar molecules and an increased ionization rate is achieved even though the driving voltage is no longer applied. Subsequently, electrons exhibit an oscillatory motion moving to the anode and then back to the cathode. This yields a second and third temperature increase. Secondary ionization is

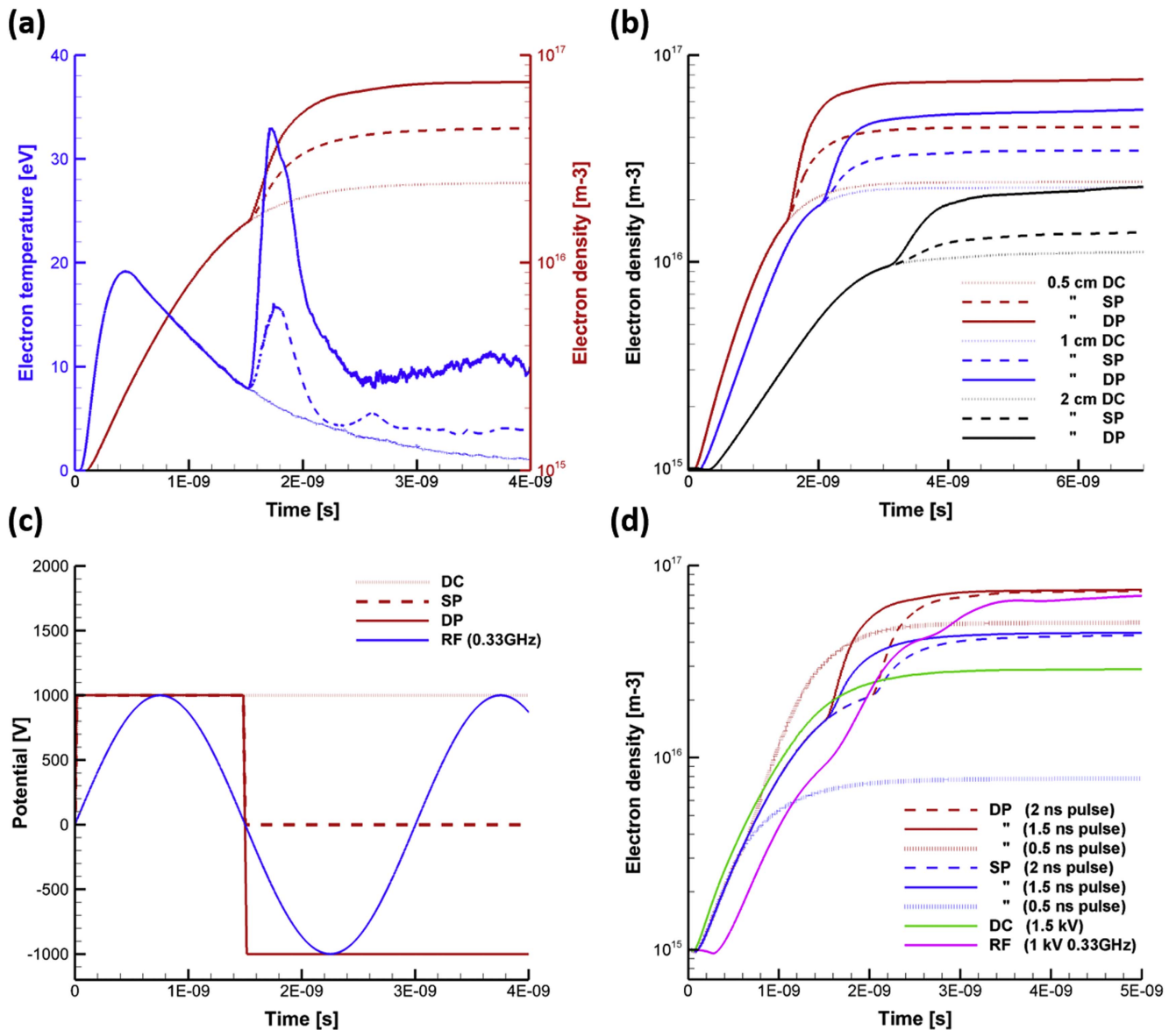


Figure 5. Transient response of averaged electron density and electron temperature in argon plasma with different voltages for DC, SP (single pulse), DP (dual pulse), and RF cases. (a) Electron density and temperature for DC (dotted line), SP (dashed line), and dual pulsed cases (solid line). (b) Electron density with 0.5, 1, 2 cm gap with DC, SP, DP cases at 1 Torr. (c) Shape of driven voltages for DC, SP, DP, and RF (0.33 GHz). (d) Electron density results for DC, SP, DP, and RF cases.

maximized when the pulse trailing edge is as steep as possible and occurs after ionization in the bulk region has saturated. A DP excitation can increase maximum density another 50%–70% above a SP excitation and in half the time of an RF sinusoidal discharge of the same period.

The results shown here are in agreement with past treatment of the field reversal phenomena and provide higher resolution analysis of the key features. In the first investigation by Raizer and Scheider [31] it was estimated that field reversal could yield a factor of 2 increase in maximum electron density. Here using a 1% pulse fall time we obtain a factor of 1.6 increase. The lower, but still significant, value is partly due to the fact the field reversal and subsequent secondary ionization is limited to a subset of the of inter-electrode gap. Analysis by Macheret *et al* [32] predicts a field

reversal that is uniform across the gap. The modeling results here show that the potential after pulse termination peaks about a quarter gap length away from the cathode. Furthermore, although the first field reversal is the most prominent, subsequent reversals have also been identified and are responsible for electron temperature increases. The DP excitation yields a factor of 3 increase in maximum electron density over a DC or long pulse discharge.

The secondary ionization phenomena described here bears some resemblance to secondary discharges observed in dielectric barrier discharge experiments [37, 38]. However, in those cases, the energy reservoir are the polarized electrodes and not only the bulk plasma itself. Liu and Neiger [37] report experiments with 20 ns rise/fall time pulses at 37.5 Torr over a 0.4 cm gap and estimate secondary ionization after pulse

termination to consume an almost equal amount of energy as the primary discharge. The stored energy in that experiment is both the dielectric electrodes and the bulk plasma from the primary discharge. The stored energy in the bulk region is capacitive in nature, so the electric field formulations presented in section 3, can be equivalently treated in terms of effective capacitance. In this context, Kozyrev *et al* [39] explore the effect of discharge gap capacitance using a zero dimensional model. The numerical results presented here show that a capacitance treatment would require a spatial dependence and the transient dielectric response of the plasma bulk region would have to be taken into account.

Overall, the results suggest that targeted pulse design can be used to condition plasma density and temperature as required for fast discharge applications. Evolution of power supply technology and electrode design suggest that the nanosecond regimes that have been explored here can be realized in the near future.

Acknowledgments

This work was supported by the Office of Naval Research (ONR) under award N00014-15-1-2526 to Georgia Institute of Technology and subcontract RG185-G1 to University of Colorado Denver and by the Defense Advanced Research Projects Agency (DARPA) under award HR0011-16-2-0031 to Georgia Institute of Technology and subcontract RH202-G1 to University of Colorado Denver.

ORCID iDs

H Y Kim  <https://orcid.org/0000-0003-3304-0722>

References

- [1] Lieberman M A and Lichtenberg A J 2015 *Principle of Plasma Discharges and Materials Processing* (New York: Wiley)
- [2] Kang S K, Kim H Y, Yun G S and Lee J K 2015 Portable microwave air plasma device for wound healing *Plasma Sources Sci. Technol.* **24** 035020
- [3] Lee M U, Lee J, Lee J K and Yun G S 2017 Corrigendum: extended scaling and paschen law for micro-sized radiofrequency plasma breakdown *Plasma Sources Sci. Technol.* **26** 034003
- [4] Iza F, Lee J K and Kong M G 2007 Electron kinetics in radio-frequency atmospheric-pressure microplasmas *Phys. Rev. Lett.* **99** 075004
- [5] Nam S K and Verboncoeur J P 2009 Theory of filamentary plasma array formation in microwave breakdown at near-atmospheric pressure *Phys. Rev. Lett.* **103** 055004
- [6] Kim H C and Lee J K 2004 Mode transition induced by low-frequency current in dual-frequency capacitive discharges *Phys. Rev. Lett.* **93** 085003
- [7] Park G Y, You S J, Iza F and Lee J K 2007 Abnormal heating of low-energy electrons in low-pressure capacitively coupled discharges *Phys. Rev. Lett.* **98** 085003
- [8] Verboncoeur J P, Alves M V, Vahedi V and Birdsall C K 1993 Simultaneous potential and circuit solution for 1D bounded plasma particle simulation codes *J. Comput. Phys.* **104** 321–8
- [9] Anderson T 2011 *Plasma Antennas* (Norwood, MA: Artech House)
- [10] Gołkowski M, Gołkowski C, Leszczynski J, Plimpton S R, Masłowski P, Foltynowicz A, Ye J and McCollister B 2012 Hydrogen-peroxide-enhanced nonthermal plasma effluent for biomedical applications *IEEE Trans. Plasma Sci.* **40** 1984–91
- [11] Plimpton S R, Gołkowski M, Mitchell D G, Austin C, Eaton S S, Eaton G R, Gołkowski C and Voskuil M 2013 Remote delivery of hydroxyl radicals via secondary chemistry of a nonthermal plasma effluent *Biotechnol. Bioeng.* **110** 1936–44
- [12] Ahn S K and Chang H Y 2008 Experimental observation of the inductive electric field and related plasma nonuniformity in high frequency capacitive discharge *Appl. Phys. Lett.* **93** 031506
- [13] Kwon H C, Won I H and Lee J K 2012 Electron heating mode transition induced by ultra-high frequency in atmospheric microplasmas for biomedical applications *Appl. Phys. Lett.* **100** 183702
- [14] Sakiyama Y, Knake N, Schröder D, Winter J, Gathen V S D and Graves D B 2010 Gas flow dependence of ground state atomic oxygen in plasma needle discharge at atmospheric pressure *Appl. Phys. Lett.* **97** 151501
- [15] Kim H Y, Kang S K, Park S M, Jung H Y, Choi B H, Sim J Y and Lee J K 2015 Characterization and effects of Ar/Air microwave plasma on wound healing *Plasma Process. Polym.* **12** 1423–34
- [16] Shiraishi T, Urushihara T and Gundersen M 2009 A trial of ignition innovation of gasoline engine by nanosecond pulsed low temperature plasma ignition *J. Phys. D: Appl. Phys.* **42** 135208
- [17] Kim H Y, Kang S K, Kwon H C, Lee H W and Lee J K 2013 Gas temperature effect on reactive species generation from the atmospheric pressure air plasma *Plasma Process. Polym.* **10** 686–97
- [18] Kim H Y, Lee H W, Kang S K, Lee H W K, Kim G C and Lee J K 2012 Modeling the chemical kinetics of atmospheric plasma for cell treatment in a liquid solution *Phys. Plasmas* **19** 073518
- [19] Kwon H C, Kim H Y, Won I H, Lee H W K, Shin H K and Lee J K 2013 Enhanced transportation of energetic electrons in dual-frequency atmospheric microplasmas *Phys. Plasmas* **20** 023506
- [20] Iza F, Kim G J, Lee S M, Lee J K, Walsh J L, Zhang Y T and Kong M G 2008 Microplasmas: source, particle kinetics, and biomedical applications *Plasma Process. Polym.* **5** 322–44
- [21] Schoenbach K H and Becker K 2016 20 years of microplasma research: a status report *Eur. Phys. J. D* **70** 29
- [22] Korolev Y D and Frank K 1999 Discharge formation processes and glow-to-arc transition in pseudospark switch *IEEE Trans. Plasma Sci.* **27** 1525–37
- [23] Savage M E, Seidel D B and Mendel C W Jr 2000 Design of a command-triggered plasma opening switch for terawatt applications *IEEE Trans. Plasma Sci.* **28** 1533–9
- [24] Schumer J W, Swanekamp S B, Ottinger P F, Comisso R J, Weber B V, Smithe D N and Ludeking L D 2001 MHD-topical transition for modeling of conduction and opening in a plasma opening switch *IEEE Trans. Plasma Sci.* **29** 479–93
- [25] Poggie J, Adamovich I, Bisek N and Nishihara M 2013 Numerical simulation of nanosecond-pulse electrical discharges *Plasma Sources Sci. Technol.* **22** 015001
- [26] Russo P, Cerri G and Vecchioni E 2011 Self-consistent analysis of cylindrical plasma antennas *IEEE Trans. Antennas Propag.* **59** 1503–11
- [27] Brelet Y, Houard A, Point G, Prade B, Arantchouk L, Carbonnel J, André Y-B, Pellet M and Mysyrowicz A 2012

- Radiofrequency plasma antenna generated by femtosecond laser filaments in air *Appl. Phys. Lett.* **101** 264106
- [28] Cohen M B, Thompson L, Opalinski N, Singletary P, Walker M, Chan C and Gotkowski M 2017 *Broadband electrically short transmitters via hi-speed time-varying antenna properties IEEE AP-S Symp. on Antennas and Propagation and USNC-URSI Radio Science Meeting*
- [29] Hill A E 1973 Continuous uniform excitation of medium-pressure CO₂ laser plasmas by means of controlled avalanche ionization *Appl. Phys. Lett.* **12** 15
- [30] Macheret S O, Shneider M N and Murray R C 2006 Ionization in strong electric fields and dynamics of nanosecond-pulse plasmas *Phys. Plasmas* **13** 023502
- [31] Raizer Y P and Shneider M N 1989 Electrodeless capacitive discharge sustained by repetitive high-voltage pulses *High Temp.* **27** 329–35
- [32] Macheret S O, Shneider M N and Mildes R B 2002 Modeling of air plasma generation by repetitive high-voltage nanosecond pulses *IEEE Trans. Plasma Sci.* **30** 1301–14
- [33] Roberto M, Smith H B and Verboncoeur J P 2003 Influence of metastable atoms in radio-frequency argon discharges *IEEE Trans. Plasma Sci.* **31** 1292–8
- [34] Vahedi V, Dipeso G, Birdsall C K, Lieberman M A and Rognlén T D 1993 Capacitive RF discharges modelled by particle-in-cell Monte Carlo simulation: I. Analysis of numerical techniques *Plasma Sources Sci. Technol.* **2** 261–72
- [35] Verboncoeur J P 2005 Particle simulation of plasmas: review and advances *Plasma Phys. Control. Fusion* **47** A231–60
- [36] Kim H C, Iza F, Yang S S, Radmilović M and Lee J K 2005 Particle and fluid simulations of low-temperature plasma discharges: benchmarks and kinetic effects *J. Phys. D: Appl. Phys.* **38** R283–301
- [37] Liu S and Neiger M 2001 Excitation of dielectric barrier discharges by unipolar submicrosecond square pulses *J. Phys. D: Appl. Phys.* **34** 1632–8
- [38] Laroussi M, Lu X, Kolobov V and Arslanbekov R 2004 Power consideration in the pulsed dielectric barrier discharge at atmospheric pressure *J. Appl. Phys.* **96** 3028–30
- [39] Kozyrev A V, Kozhevnikov V Y and Semeniuk N S 2015 Zero-dimensional theoretical model of subnanosecond high-pressure gas discharge *IEEE Trans. Plasma Sci.* **43** 4077–80